α-$RuCl_3$/Polymer Nanocomposites: The First Group of Intercalative Nanocomposites with Transition Metal Halides

Lei Wang,[†] Melissa Rocci-Lane,[‡] Paul Brazis,[‡] Carl R. Kannewurf,[‡] Young-Il Kim,[§] Woo Lee,[§] Jin-Ho Choy,[§] and Mercouri G Kanatzidis*,[†]

Contribution from the Department of Chemistry and Center for Fundamental Materials Research, Michigan State University, East Lansing, Michigan 48824, Department of Electrical and Computer Engineering, Northwestern University, Evanston, Illinois 60208, and Department of Chemistry and National Research Laboratory, College of Natural Sciences, Seoul National University, Seoul 151-742, Korea

Received December 21, 1999

Abstract: Different types of polymers can be intercalated into α-$RuCl_3$ with different synthetic methodologies. Polyaniline/α-$RuCl_3$ nanocomposite was prepared by the in situ redox intercalative polymerization method, in which α-$RuCl_3$ was exposed to an aniline/acetonitrile solution in open air. Water-soluble polymers such as poly(ethylene oxide), poly(vinyl pyrrolidone), and polyethylenimine were intercalated by an encapsulative precipitation method using monolayer suspensions of α-$RuCl_3$. A modification of this method led to insertion of polypyrrole. Monolayer suspensions of α-$RuCl_3$ can be prepared from Li_xRuCl_3 ($x \sim 0.2$). The latter is produced by the reaction of α-$RuCl_3$ with 0.2 equiv of $LiBH_4$. The polymer insertion is topotactic and does not cause structural changes to the host. The metal chloride layers in these materials possess mixed valency. The reduction and polymer intercalation of α-$RuCl_3$ alters the intralayer and interlayer Ru^{3+} (low spin d^5) magnetic coupling, so that interesting magnetic properties appear in the nanocomposites. In addition, the reduction brings in free hopping electrons to the $RuCl_3$ layers and the polymer intercalation builds up new electronic or ionic conducting channels in the galleries, so that the charge transport properties are changed dramatically. For example, Li_xRuCl_3 shows an electrical conductivity 3 orders of magnitude higher than pristine α-$RuCl_3$ at room temperature and $Li_x(PEO)_yRuCl_3$ has an ion conductivity comparable with the best (lithium salt)−polymer electrolytes. For a comprehensive understanding of the structure of the representative nanocomposite $Li_x(PEO)_yRuCl_3$, the arrangement of polymer chains inside the galleries was explored with analysis of its one-dimensional (00*l*) X-ray diffraction pattern. Calculated electron density maps along the stacking *c*-axis lead to a structural model that fills each gallery with two layers of polymer chains exhibiting a conformation found in type-II PEO−$HgCl_2$. The most consistent PEO arrangement in the gallery generates oxygen-rich channels in the middle of the gallery in which the Li ions can reside. The new nanocomposites were characterized with thermogravimetric analysis, infrared spectroscopy, powder X-ray diffraction, magnetic measurements, as well as electrical and ionic conductivity and thermopower measurements.

Introduction

The combination of two extremely different components, at the molecular level, provides an avenue to designing new nanocomposite hybrid materials as well as the ability to modulate the properties of one or more of the components.[1] In some circumstances, it is also a unique way to generate materials which have special properties that are unknown in the individual constituents.[2] Intercalation compounds with polymers as the guest species are an important class of nanocomposite materials.[3] Intercalative polymer hybrids have advantages over their small molecular analogues in compositional stability and mechanical strength, which make them more suitable for applications. As a result of recent efforts, a large variety of intercalative nanocomposites has been prepared using hosts from most major classes of layered inorganic compounds, i.e., clays, layered transition metal chalcogenides, metal oxides, metal phosphates, and metal thiophosphates.[4]

Layered transition metal halides, in contrast to layered metal chalcogenides,[5] oxides,[6] and thiophosphates,[7] have not received much attention in the study of intercalation, because most of them are not very stable, even under mild conditions, for soft chemical reactions. Hydrolysis, dissolution, and other decomposition reactions are often common properties of this group

[†] Michigan State University.
[‡] Northwestern University.
[§] Seoul National University.

(1) Leroux, F.; Koene, B. E.; Nazar, L. F. *J. Electrochem. Soc.* **1996**, *143* (9), L181. (b) Leroux, F.; Goward, G.; Power, W. P.; Nazar, L. F. *J. Electrochem. Soc.* **1997**, *144*, 3886.

(2) Wang, Y.; Herron, N. *Science* **1996**, *273* (5275), 632.

(3) (a) O'Hare, D. In *Inorganic Materials*; Bruce, D. W., O'Hare, D., Eds.; John Wiley & Sons Ltd: New York, 1992; p 164. (b) Ruiz-Hitzky, E. *Adv. Mater.* **1993**, *5*, 334. (c) Alberti, G.; Bein, T., Eds. *Comprehensive Supramolecular Chemistry*; Elsevier Science Ltd: New York, 1996; Vol. 7. (d) Giannelis, E. P. *Adv. Mater.* **1996**, *8*, 29.

(4) (a) Giannelis, E. P. *Adv. Mater.* **1996**, *8*, 29. (b) Ruiz-Hitzky, E.; Aranda, P.; Casal, B.; Galván, J. C. *Adv. Mater.* **1995**, *7*, 180.

(5) (a) Hsu, C.-H.; Labes, M. M.; Breslin, J. T.; Edmiston, D. J.; Winter, J. J.; Leupold, H. A.; Rothwarf, F. *Nature, Phys. Sci.*, **1973**, *246* (155), 122. (b) Kanatzidis, M. G.; Bissessur, R.; DeGroot, D. C.; Schindler, J. L.; Kannewurf, C. R. *Chem. Mater.* **1993**, *5*, 595.

(6) (a) Liu, Y.-J.; DeGroot, D. C.; Schindler, J. L.; Kannewurf, C. R.; Kanatzidis, M. G. *Adv. Mater.* **1993**, *5*, 369. (b) Nazar, L. F.; Zhang, Z.; Zinkweg, D. *J. Am. Chem. Soc.* **1992**, *114*, 6239.

(7) Lagadic, I.; Léaustic, A.; Clément, R. *J. Chem. Soc., Chem. Commun.* **1992**, 1396.

10.1021/ja9944610 CCC: $19.00
Published on Web 06/29/2000

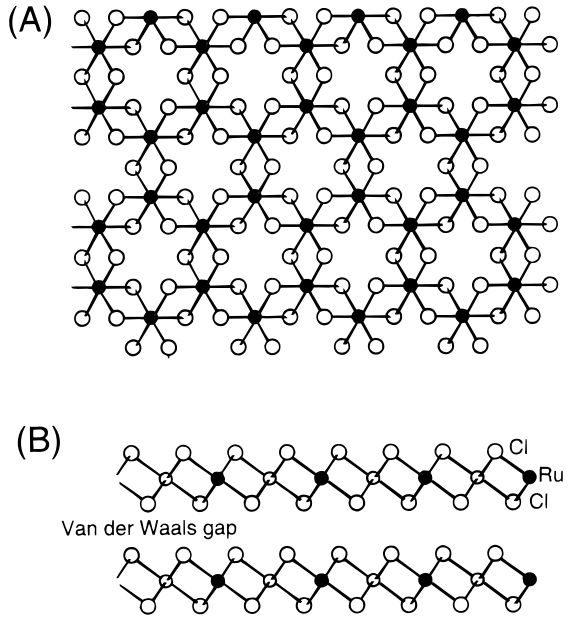

Figure 1. The layered structure of α-$RuCl_3$. The coordination environment of the Ru atoms is octahedral. (A) View down the *c*-axis. (B) View parallel to the layers.

of materials. α-$RuCl_3$ is a notable exception and is very stable under these conditions.

α-$RuCl_3$ has a lamellar structure that can be regarded as defect CdI_2 type, see Figure 1. Intercalation chemistry of α-$RuCl_3$ has been reported with the insertion of simple cations and neutral polar molecules.[8] Cations can be intercalated reductively or through ion-exchange, while neutral polar molecules can be incorporated through solvent exchange. These properties are similar to those of layered chalcogenides and oxides such as TiS_2, 2H-TaS_2, and MoO_3, suggesting the possibility of intercalating polymers in this material. In fact, as we describe here, α-$RuCl_3$ behaves as an excellent polymer-intercalation host. It exhibits affinity for various polymers and is compatible with several of the existing polymer intercalation methods. For example, α-$RuCl_3$/polyaniline (α-$RuCl_3$/PANI) nanocomposites were synthesized with in situ redox intercalative polymerization,[9] while soluble polymers such as poly(ethylene oxide) (PEO), poly(vinyl pyrrolidone) (PVP), and poly(ethylene-imine) (PEI) are intercalated through encapsulative coprecipitation[10] of polymers and α-$RuCl_3$ from solutions of exfoliated α-$RuCl_3$. A modification of the second method, in situ polymerization coupled with encapsulative precipitation[11] from suspensions of exfoliated α-$RuCl_3$, can be used to insert intractable polymers such as polypyrrole (PPY). Here we report in detail the insertion or encapsulation of polymers into α-$RuCl_3$ to produce a new group of lamellar nanocomposites with diverse physicochemical properties. Two different types of polymers were examined, conjugated and conventional nonconjugated systems. The former include polyaniline (PANI) and polypyrrole (PPY) whereas the latter involved poly(ethylene oxide) (PEO), poly(ethylene-imine) (PEI) and poly(vinylpyrrolidone) (PVP). The Li/PEO/ $RuCl_3$ system exhibits mixed electronic/ionic conductivity with a very substantial ionic charge transport component.

Experimental Section

1. Reagents. $LiBH_4$ (95%), PEO (100 000), PVP (10 000), and PEI (25 000) were purchased from Aldrich Chemical Co., Inc. After the polymers were dissolved, the polymer solutions were filtered to remove insoluble residues. Aniline and pyrrole were purchased from Aldrich and Mallinckrodt Inc., respectively, and were distilled before use.

2. Syntheses and Reactions.(a) Preparation of α-$RuCl_3$. α-$RuCl_3$ was synthesized as described in the literature.[12] The setup for the reaction (the gas supply, outlet tubing and the quartz reaction tube) was first purged with nitrogen overnight. A sample of 10 g of Ru metal powder spread in an alumina boat was reacted with flowing mixed Cl_2 and CO gases at 800 °C for 8 h. The ratio of Cl_2 to CO gas was adjusted to about 1:2 or 1:3 and the flow was set at approximately 60−120 mL/min. The gas began to flow before heating and was turned off after the reaction tube cooled to about 50 °C. Very thin platelike crystals of α-$RuCl_3$ were collected from the cooler end of the tube (down stream) in a yield that exceeded 40%.

(b) Synthesis of $(PANI)_xRuCl_3$. A sample of 0.1 g of α-$RuCl_3$ in 10 mL of 4% aniline/acetonitrile solution was stirred in open air for 1 week. The product was washed with copious acetonitrile and dried in a vacuum. Elemental analysis, done by Quantitative Technologies Inc., gave 15.33% C, 1.43% H, 3.11% N, which suggests the formula $(PANI)_{0.57}(H_2O)_{0.50}RuCl_3$ (calculated 15.3% C, 1.43% H, 2.97% N). The above formula contains 22 wt % water as determined from thermogravimetric analysis (TGA) measurements.[13] The formula $(PANI)_xRuCl_3$ can vary from $x \sim 0.55$ to 0.7 depending on preparation conditions.

(c) Synthesis of Li_xRuCl_3 and Preparation of $RuCl_3$ Monolayer Suspensions. In a typical reaction, 18 mmol of α-$RuCl_3$ was mixed with 3.6 mmol of $LiBH_4$ in 40 mL of anhydrous ether under N_2 atmosphere for 3 days. The product was collected by filtration, washed with anhydrous ether, and pumped to dryness. It was stored in a glovebox under N_2 atmosphere. The product is designated as Li_xRuCl_3, where $x \approx 0.2$. An aqueous $[RuCl_3]^{x-}$ monolayer suspension was prepared simply by stirring Li_xRuCl_3 in water for 30 min. The value of x was determined with ICP analysis. Compositions with $x > 0.2$ are possible but they were not explored in this work.

(d) Synthesis of $Li_x(PEO)_yRuCl_3$, $Li_x(PEI)_yRuCl_3$, and $Li_x(PVP)_yRuCl_3$. In the preparation of PEO and PVP nanocomposites, a sample of 40 mL of 0.5 wt % Li_xRuCl_3 monolayer suspension (0.96 mmol of Li_xRuCl_3) was mixed with 40 mL of polymer solution containing 3 mmol repeat-units of polymer. The mixture was stirred for 2 days in ambient atmosphere. The nanocomposites of PEO and PVP are still colloidal, and have to be collected from very concentrated solutions. Therefore, the reaction mixture was condensed to less than 20 mL under vacuum before it was poured into an organic solvent (e.g. ether) to precipitate the product. Acetonitrile and 2-propanol were used as solvents for PEO and PVP, respectively. In the preparation of the PEI nanocomposite, the sample of 40 mL of 0.5 wt % Li_xRuCl_3 monolayer suspension was mixed with 40 mL of PEI solution containing 7 mmol repeat-units of polymer. The PEI nanocomposite precipitated

(8) (a) Schöllhorn, R.; Steffen, R.; Wagner, K. *Angew. Chem., Int. Ed. Engl.* **1983**, *22*, 555. (b) Steffen, R.; Schöllhorn, R. *Solid State Ionics* **1986**, *22*, 31. (c) Nonte, W.; Lobert, M.; Müller-Warmuth, W.; Schöllhorn, R. *Synth. Met.* **1989**, *34*, 665.

(9) Wang, L.; Brazis, P.; Rocci, M.; Kannewurf, C. R.; Kanatzidis, M. G. *Chem. Mater.* **1998**, *10*, 3298.

(10) The method of encapsulative precipitation from solutions of exfoliated lamellar solids has be applied to MoS_2, MoO_3, TaS_2, and $NbSe_2$: (a) Bissessur, R.; Kanatzidis, M. G.; Schindler, J. L.; Kannewurf, C. R. *J. Chem. Soc., Chem. Commun.* **1993**, 1582. (b) Wang, L.; Schindler, J.; Kannewurf, C. R.; Kanatzidis, M. G. *J. Mater. Chem.* **1997**, *7*, 1277. (c) Wang, L.; Schindler, J.; Kannewurf, C. R.; Kanatzidis, M. G. Manuscript in preparation. (d) Tsai, H.-L.; Schindler, J. L.; Kannewurf, C. R.; Kanatzidis, M. G. *Chem. Mater.* **1997**, *9*, 875.

(11) The method of in situ polymerization coupled with encapsulative precipitation has been applied to MoS_2, MoO_3, and WS_2: (a) Wang, L.; Schindler, J. L.; Thomas, J. A.; Kannewurf, C. R.; Kanatzidis, M. G. *Chem. Mater.* **1995**, *7*, 1753. (b) Kerr, T. A.; Wu, H.; Nazar, L. F. *Chem. Mater.* **1996**, *8*, 2005. (c) Wang, L. Intercalated Polymer-Layered Inorganic Nanocomposites, Ph.D. Dissertation, 1999, Department of Chemistry, Michigan State University.

(12) Brauer, G. *Handbook of Preparative Inorganic Chemistry*; Academic Press Inc.: New York, 1965; Vol. 2, p 1597.

(13) TGA indicated a total loss of 48.2% in oxygen flow at temperatures up to 650 °C. By comparison, α-$RuCl_3$ under the same conditions loses 33.07% of its weight and converts to RuO_2. The amount of organics and water inside the nanocomposite was determined assuming the final product is RuO_2. The amount of intercalates in $Li_x(PEO)_yRuCl_3$, $Li_x(PVP)_yRuCl_3$, and $Li_x(PEI)_yRuCl_3$ was determined similarly.

out from water immediately upon mixing. It was collected with centrifugation after the suspension was stirred for 2 days. The nanocomposites were dried under vacuum. The compositions of the three nanocomposites were $Li_x(PEO)_{1.5}RuCl_3$ ($x \sim 0.2$), $Li_x(PVP)_{2.2}$-$RuCl_3$ ($x \sim 0.2$), and $Li_x(PEI)_{4.6}RuCl_3$ according to TGA measurements under oxygen flow.[13] These compositions gave satisfactory C, H, N elemental analyses. The amount of Li was determined with inductively coupled plasma spectroscopy (ICP).

(e) Synthesis of $(PPY)_xRuCl_3$. A sample of 0.45 g (6.7 mmol) of pyrrole was dissolved in 40 mL of water and mixed with 40 mL of aqueous suspension which contained 0.20 g (0.96 mmol) of Li_xRuCl_3. The mixture was cooled in an ice bath before the dropwise addition of a cold 10 mL aqueous solution of 0.11 g (0.67 mmol) of $FeCl_3$. The mixture was stirred in a closed, ice-cooled flask for 24 h. The product was collected by centrifugation, washed with copious water, and dried in air and under vacuum. Elemental analysis gave 13.88% C, 1.32% H, and 3.95% N. This corresponds to $(PPY)_{0.77}(H_2O)_{0.60}RuCl_3$ (calculated 13.78% C, 1.31% H, and 4.01% N). The product did not contain Li. TGA measurements (in air) showed that the material lost 50.2% (theoretical 50.4%) of its weight in oxygen at temperatures higher than 450 °C. X-ray powder patterns of the final residue indicated pure RuO_2.

3. Physicochemical Measurements. (a) Instrumentation. X-ray diffraction (XRD) powder patterns were obtained on a Rigaku Ru-200B X-ray diffractometer, at 45 kV and 100 mA, with a scintillation counter detector and a graphite monochromator to produce a Cu Kα beam ($\lambda = 1.54184$ Å). A continuous scanning mode with a speed of 1 deg/min in 2θ and an increment of 0.05° was chosen for general purpose spectra. For 1-D ED calculations, we obtained XRD data from highly oriented samples and a stepwise scanning mode with 0.1° per step.

Infrared (IR) spectra were collected on solid samples as pressed KBr pellets using a Nicolet IR/42 spectrometer with a 2.0 cm^{-1} resolution. A typical 64 scans were applied for each sample. Thermal gravimetric analysis (TGA) was performed with a Shimadzu TGA-50 under an oxygen flow of 46 mL/min. The heating rate was 10 deg/min.

Scanning electron microscopy (SEM) and energy-dispersive X-ray microanalysis (EDS) were done with a JEOL-JSM 35 CF microscope at an accelerating voltage of 15 and 20 kV, respectively. Samples were mounted on a sample stab with conductive tape. Electron diffraction experiments were performed with a JEOL-100CX transmission electron microscope (TEM) operating at 120 kV.

Magnetic susceptibility measurements were done with a Quantum Design MPMS2 SQUID magnetometer in the temperature region of 4−300 K. Samples were sealed in low-density polyethylene (LDPE) bags under a nitrogen atmosphere. The magnetic moments of the bags were acquired and subtracted from the data. To obtain the magnetic susceptibility χ_{molar}, the diamagnetic susceptibility χ_d and χ_{TIP} were subtracted from the total susceptibility. The χ_d was derived by adding up the diamagnetic susceptibility of each component, which was obtained from the literature.[14]

Electrical conductivity data were obtained with a computer-automated system described elsewhere.[15]

(b) X-ray Diffraction and One-Dimensional Electron Density Maps. One-dimensional electron density (1-D ED) maps were calculated from XRD data collected from highly oriented film samples in a stepwise scanning mode. These film samples were made by casting aqueous nanocomposite solutions so that the basal planes of the $RuCl_3$ layers restacked parallel to the substrate. Several layers of a film were loaded in the sample plate so as to obtain maximum diffraction intensity. Immediately before the X-ray experiments, the samples were pumped at 75 °C for 3 days to remove excess water from the nanocomposite. This procedure ensures that the sample has only one phase with a single basal spacing. The X-ray patterns were collected under a nitrogen atmosphere to prevent absorption of moisture, which causes peak broadening and drifting. In the measurements, slits for different beam width, as well as different data collection times, were used for different 2θ ranges, to achieve a compromise between peak broadening, peak intensity, and experiment time. Specifically, 0.5° slits and a data collection time of 12 s per step were chosen for measurements in the range from 2° to about 29°; 1.0° slits and 60 s per step between 16° and 71°; 2.0° slits and 60 s per step between 57° and 83.5°; and 4.0° slits and 90 s per step from 72° to 136°. The step width was kept the same (0.1°) for the entire 2θ range.

A full range XRD pattern ($2° \le 2\theta \le 136°$) was obtained by merging the data from the different 2θ ranges and scaling them based on the overlapped regions. The overlapped data regions had at least two peaks in common. The full data set was put into the XRD analysis program PEAKOC[16] to calculate the integrated peak area of each 00*l* reflection. In pattern analysis, 00*l* peaks were fit with the split-pseudo-Voigt function with a linear background subtraction for each peak. The integrated peak area of the 00*l* peaks was used as their intensity. The methodology used has been described in detail elsewhere.[17] A FORTRAN program was written to calculate the 1-D ED map. The signs (phases) of the structure factors were assigned based on the signs of the corresponding structure factors of the $RuCl_3$ framework alone. This reasonably assumes that the scattering contribution from the intercalated polymer is relatively small compared to that of the $RuCl_3$ component. After the model for the structure was established, the sign of the F_l was checked by recalculating F_l^{calc} from the scattering of all atoms including those of the polymer.

(c) Impedance Spectroscopy Measurements. Impedance spectroscopy measurements were carried out on a Hewlett-Packard HP4192A low-frequency impedance analyzer to probe the impedance $|Z^*|$ and the phase angle ϕ. Samples were pressed into disks under 50 kg/m^2 pressure and assembled between two stainless steel electrodes in an air-proof cell under a nitrogen atmosphere. The range of frequency ω used in the measurements was 5−13 MHz. The cell was heated in a silicon oil bath. Interpretation of the impedance spectra was made by fitting the data with equivalent circuits. Nonlinear least-squares fitting, which minimizes the sum $\sum_\omega |Z^*|^{-1}\{(Z'_{exp} - Z'_{sim})^2 + (Z''_{exp} - Z''_{sim})^2\}$, was used to determine the values of the electrical elements in the equivalent circuit.[18]

Results and Discussion

In this section, the synthesis and characterization of several families of hybrid polymer/$RuCl_3$ lamellar intercalative nanocomposites are described. Next the structural arrangement of the PEO member is explored and compared with those of other PEO systems. Finally, it is shown that the conjugated polymers are crucial to achieving high electronic conductivities whereas in the Li/PEO/$RuCl_3$ case the ionic transport is greatly enhanced, compared to that of Li/$RuCl_3$, and is as good as some of the best Li/PEO electrolyte salts.

1. Preparation of $(PANI)_xRuCl_3$ by in Situ Redox Intercalative Polymerization. The in situ redox intercalative polymerization reaction is the most direct method to intercalate conductive polymers in open-framework hosts. Its topotactic character least disturbs the crystalline structure of the host. In the case of FeOCl/polyaniline, even single crystals of the nanocomposite could be obtained.[19] This type of reaction requires a strongly oxidizing host to provide a driving force to pull electrons from the monomers and oxidize them into polymers. In addition, the host should be able to distribute

(14) (a) Selwood, P. W. *Magnetochemistry*, 2nd ed.; Interscience Publishers: New York, 1956; p 78. (b) Drago, R. S. *Physical Methods for Chemists*; 2nd ed.; Saunders College Publishing: Philadelphia/San Diego/New York, 1992; Chapter 11. (c) Epstein, A. J.; Ginder, J. M.; Richter, A. F.; MacDiarmid, A. G. In *Conducting Polymers*; Alcácer, L., Ed.; D. Reidel Publishing Company: Dordrecht, The Netherlands, 1986; p 121.

(15) Lyding, J. W.; Marcy, H. O.; Mark T. J.; Kannewurf, C. R. *IEEE. Trans. 1nstrum. Meas.* **1988,** *37*, 76.

(16) PEAKOC is an XRD powder pattern analysis computer program provided by Inel Inc. (Mail Adress in U.S.A.: P.O. Box 147, Stratham, NH 03885.)

(17) Leung, S. Y.; Dresselhaus, M. S.; Underhill, C.; Krapchev, T.; Dresselhaus, G.; Wuensch, B. J. *Phys. Rev. B-Cond. Matter* **1981**, *24* (6), 3505−3518

(18) (a) Choy, J. H.; Park, N. G.; Kim, Y. I.; Hwang, S. H.; Lee, J. S.; Yoo, H. I. *J. Phys. Chem.* **1995**, *99*, 7845. (b) Lee, J. S.; Yoo, H. I. *Solid State Ionics* **1994**, *68*, 139.

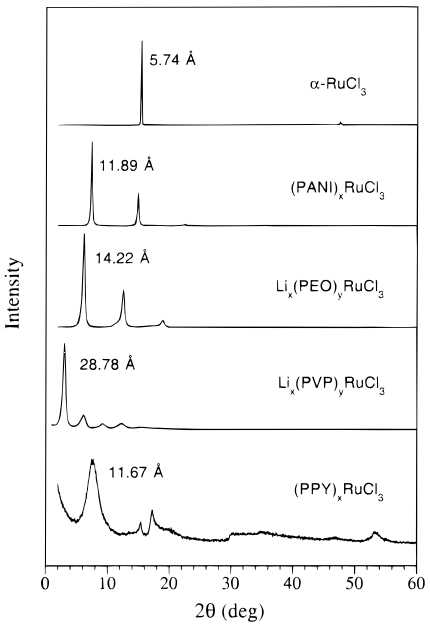

Figure 2. X-ray diffraction patterns (reflection mode) of α-$RuCl_3$ and nanocomposites.

efficiently those electrons throughout the structure. Because of the scarcity of such highly oxidizing and conducting hosts, the reaction has been limited to FeOCl,[19] V_2O_5,[20] and $VOPO_4$.[21] Now we have discovered that α-$RuCl_3$ is also a suitable host, and can form intercalative nanocomposites with polyaniline.

The reaction of an aniline/CH_3CN solution with α-$RuCl_3$ in air results in the formation of polyaniline (PANI) within the gallery space of $RuCl_3$. The reflection-mode powder X-ray diffraction (XRD) patterns of the product show a 6.2 Å increase in the separation of the $RuCl_3$ layers, see Figure 2. This expansion is reasonable for insertion of a monolayer of PANI molecules, and comparable to the 5.94 Å observed in $(PANI)_xFeOCl$[19] and 5.2 Å in $(PANI)_xV_2O_5$.[20] The transmission-mode powder XRD patterns show that the *hk*0 reflections of $(PANI)_xRuCl_3$ remain the same as those of α-$RuCl_3$, indicating that the inorganic host structure (i.e. its framework) is preserved. This result is also supported by electron diffraction experiments, which provide essentially identical two-dimensional *hk*0 diffraction patterns for $(PANI)_xRuCl_3$ and α-$RuCl_3$.

The formation of polyaniline between the $RuCl_3$ layers is supported by IR spectroscopy. Almost all peaks in the IR spectra of $(PANI)_xRuCl_3$ are associated with polyaniline (emeraldine salt) and only a few with the anilinium cation (at 744 and 687 cm^{-1}), see Figure 3A. The peaks corresponding to the polymer are much more intense than those of anilinium. Heating the product at 120 °C in air for 5 days removes all anilinium peaks. The appearance of monomer peaks implies that the polyaniline formed in the galleries does not have very high molecular weight. This is reasonable since both the concentration and mobility of the aniline in the gallery are limited. We speculate the polymer MW to be ~5000, as was found in the $(PANI)_x$-FeOCl system.

In the process of intercalation, a fraction of Ru^{3+} centers is reduced to Ru^{2+} giving a mixed-valence compound. The Ru^{2+} centers are very stable due to their low spin, diamagnetic d^6 character. The d^6 electron configuration maximizes the Ligand Field Stabilization Energy (LFSE) and this probably acts as a powerful driving force for the oxidation of aniline. As has been demonstrated in the intercalative polymerization of aniline in FeOCl and V_2O_5, the presence of oxygen is key to a successful outcome of the reaction. This was verified by control experiments where in the absence of air or oxygen no intercalation reaction occurred after 23 days. Ambient oxygen serves as an important electron acceptor so that it relieves the pressure on the host to accept and distribute large numbers of electrons which could destabilize the host structure.

2. Nanocomposites of α-$RuCl_3$ with Water Soluble Polymers. To prepare nanocomposites with water soluble polymers, the method of encapsulative precipitation from solutions of exfoliated lamellar solids was used.[6,10,22] To a stable and concentrated aqueous Li_xRuCl_3 monolayer suspension, water-soluble polymers PEO, PVP, and PEI were added and subsequently encapsulated. The XRD reflectivity patterns of the products show that the interlayer spacings of $Li_x(PEO)_yRuCl_3$, $Li_x(PVP)_yRuCl_3$, and $Li_x(PEI)_yRuCl_3$ increase by 8.5, 23.0, and 3.6 Å, respectively, see Figure 2.[23] The existence of PEO, PVP, and PEI in the nanocomposites was confirmed by IR spectroscopy, see IR spectra C and D of $Li_x(PEO)_yRuCl_3$ and $Li_x(PVP)_y$-$RuCl_3$ in Figure 3.

3. α-$RuCl_3$/Polypyrrole Nanocomposites. The exfoliating property of Li_xRuCl_3 offers the possibility to synthesize nanocomposites with insoluble polymers, by in situ polymerization−encapsulative precipitation.[11] In this method, a solution of a suitable monomer (such as pyrrole) is mixed with an exfoliated suspension of the inorganic host. When an initiator is added, the polymerization causes the coprecipitation of the polymer and host monolayers, forming a nanocomposite. This happens because the growing polymer (in this case polypyrrole) is a positively charged species and adheres to the negatively charged inorganic layers mainly due to electrostatic forces. The initiator in this case is the Fe^{3+} ions.

The formation of lamellar $(PPY)_xRuCl_3$ ($x \sim 0.7$) is indicated by XRD patterns which show basal spacings of ~11.7 Å, see Figure 2. The existence of the conductive form of polypyrrole in the galleries is confirmed by its characteristic IR spectrum, which exhibits peaks at 1541, 1314, 1150 1043, and 963 cm^{-1},[24] see Figure 3B. The 6 Å spacing between the $RuCl_3$ layers corresponds to a monolayer of polypyrrole arranged with its pyrrole rings inclined ~40° to the $RuCl_3$ layers. This situation is similar to that of $(PPY)_xMoS_2$ obtained from pyrrole-rich conditions.[11b,c] The packing density of polypyrrole in $(PPY)_x$-$RuCl_3$, 0.77 pyrrole-unit per $RuCl_3$, is comparable to that in $(PPY)_xMoS_2$ prepared under similar conditions, 0.50 pyrrole-unit per MoS_2.[25]

In the reaction to form $(PPY)_{0.77}RuCl_3$, only 0.7 equiv of $FeCl_3$ was used, which could oxidize, at maximum, ~0.35 equiv

(19) Wu, C.-G.; DeGroot, D. C.; Marcy, H. O.; Schindler, J. L.; Kannewurf, C. R.; Bakas, T.; Papaefthymiou, V.; Hirpo, W.; Yesinowski, J. P.; Liu, Y.-J.; Kanatzidis, M. G. *J. Am. Chem. Soc.* **1995**, *117*, 9229.

(20) Wu, C.-G.; Marcy, H. O.; Kannewurf, C. R.; Kanatzidis, M. G. *J. Am. Chem. Soc.* **1989**, *111*, 4139.

(21) Nakajima, H.; Matsubayashi, G. *J. Mater. Chem.* **1994**, *4* (8) 1325.

(22) Bissessur, R.; Schindler, J. L.; Kannewurf, C. R.; Kanatzidis, M. G. *Mol. Cryst. Liq. Cryst.* **1993**, *245*, 249−254

(23) Electron diffraction experiments showed that the exfoliated single $RuCl_3$ layers have the same hexagonally symmetric *hk*0 diffraction pattern as α-$RuCl_3$. The same electron diffraction pattern was also observed in $(PANI)_xRuCl_3$, suggesting no change in intralayer structure during intercalation and thus a truly topotactic process.

(24) Polypyrrole exhibits peaks at 1540, 1300, 1150, 104, and 900 cm^{-1}: Kang, E. T.; Neoh, K. G.; Tan, T. C.; Ong, Y. K. *J. Macromol. Sci.-Chem.* **1987**, *A24* (6), 631.

(25) The $(PPY)_xMoS_2$, prepared under similar conditions, has $x \sim 0.5$. Considering that the unit area of $RuCl_3$ is 1.75 times that of MoS_2, the amount of polypyrrole in the galleries is quite comparable. (For a single MoS_2 layer one unit cell contains one Mo and two S atoms; its *a*-axis dimension is 3.159 Å. By comparison, for one unit cell of two Ru and six Cl atoms has 5.87 Å as its *a*-axis dimension.)

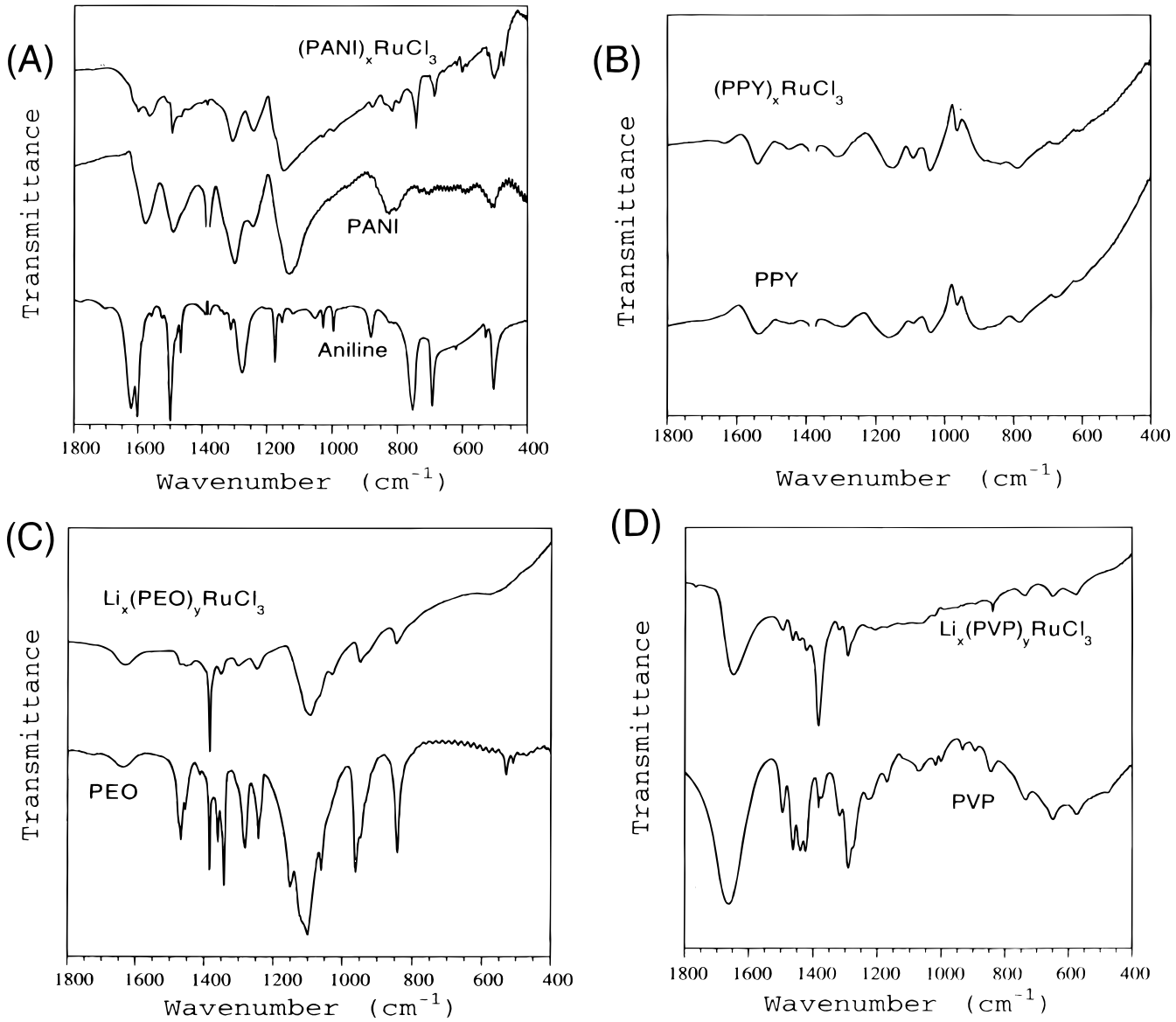

Figure 3. Infrared spectra: (A) $(PANI)_xRuCl_3$, PANI, and aniline; (B) $(PPY)_xRuCl_3$ and PPY; (C) $Li_x(PEO)_yRuCl_3$ and PEO; and (D) $Li_x(PVP)_y$-$RuCl_3$ and PVP. (The peak at 1385 cm^{-1} is due to an impurity in KBr.)

of pyrrole to polypyrrole. Therefore, the amount of polypyrrole is greater than what would be expected if $FeCl_3$ alone were the oxidant. This discrepancy is explained by the fact that the ambient oxygen participates in the reaction as an electron acceptor, as discussed above. It has been proven that ambient oxygen can oxidize and polymerize pyrrole and its oligomers when $FeCl_3$ is present as a catalyst.[26] Ambient oxygen has been shown to be the ultimate electron acceptor in the formation of $(PPY)_xV_2O_5{\cdot}nH_2O$ nanocomposites as well.[27]

For comparison we also tried the in situ redox intercalative polymerization to prepare a $RuCl_3$/PPY nanocomposite. This procedure uses α-$RuCl_3$ rather than an exfoliated suspension. When α-$RuCl_3$ was stirred in an aqueous pyrrole solution[28] in open air, intercalation occurred in two weeks to form a product with 11.2 Å basal spacing. However, in contrast to the PANI/$RuCl_3$ system, IR spectroscopy showed that the polymer formed inside the gallery was not ordinary polypyrrole but a highly defective form. Further investigations were not performed.

4. Charge Transport Properties. The insertion of polymers or Li causes large changes in the properties of α-$RuCl_3$. Because of the formation of Ru^{2+} centers, the resulting materials are now mixed-valent compounds with both Ru^{2+} and Ru^{3+} in the structure. This provides free hopping electrons between the metal atoms and explains the relatively high electrical conductivity of Li_xRuCl_3 ($x \sim 0.2$) at room temperature of ~0.3 S/cm, about 3 orders of magnitude higher than that of pristine α-$RuCl_3$, 5×10^{-4} S/cm.[29] Intercalation of insulating polymers reduces the conductivity (with respect to that of Li_xRuCl_3) to 4.5×10^{-3} and 1.7×10^{-3} S/cm for PEO and PVP, respectively. The charge transport in these two materials is substantially enhanced by the presence of *conductive* polymers. Thus $(PANI)_xRuCl_3$ shows a room temperature conductivity of ~1 S/cm, whereas $(PPY)_xRuCl_3$ shows 23 S/cm.

Variable-temperature measurements on pressed pellets reveal that the electrical conductivities of α-$RuCl_3$, Li_xRuCl_3 ($x \sim 0.2$),

(26) Toshima, N.; Ihata, O. *Synth. Met.* **1996**, *79*, 165.

(27) (a) Wu, C. G.; DeGroot, D. C.; Marcy. H. O.; Schindler, J. L.; Kannewurf, C. R.; Liu, Y. J.; Hirpo, W.; Kanatzidis, M. G. *Chem Mater* **1996**, *8* (8) 1992. (b) Wu, C. G. Ph.D. Dissertation, Michigan State University, 1992.

(28) The choice of solvent is important. For example, a pyrrole/CH_3CN solution significantly decreases the reaction rate and does not produce single-phase $(PPY)_xRuCl_3$ even after one month.

(29) Binotto, L.; Pollini, I.; Spinolo, G. *Phys. Status Solidi B* **1971**, *44*, 245.

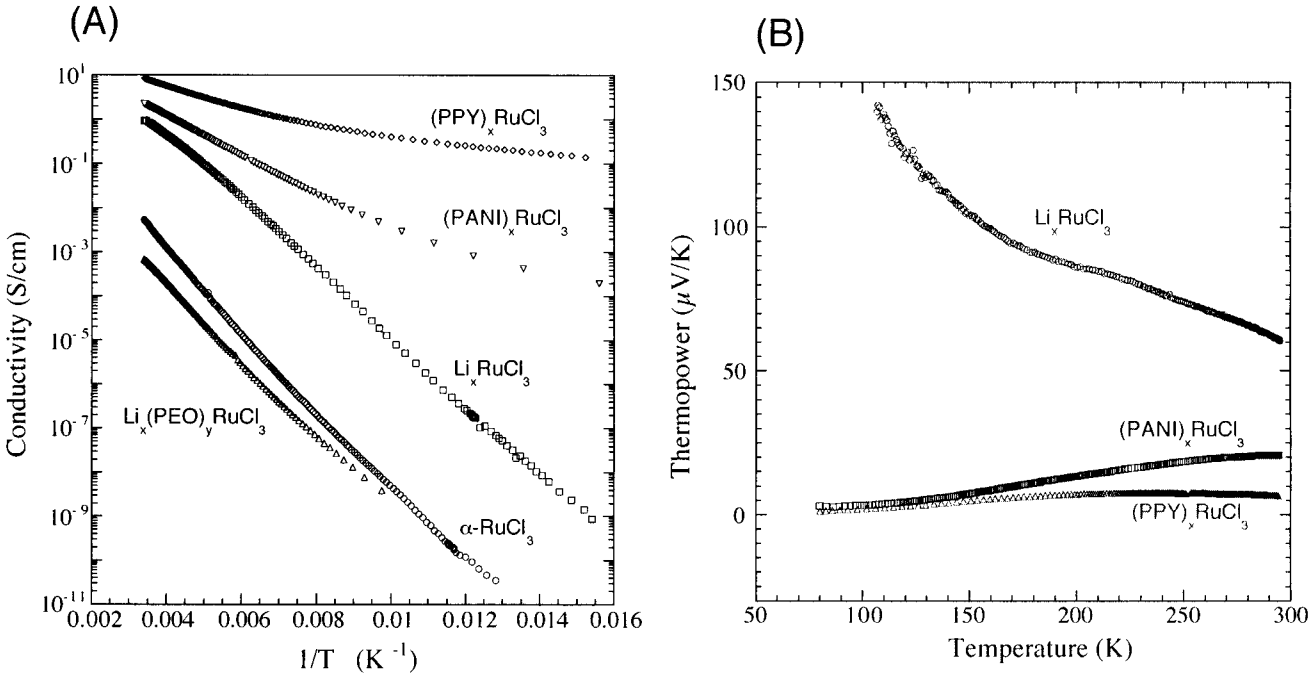

Figure 4. (A) Variable-temperature electrical conductivity measurements for pressed pellets of α-$RuCl_3$ and nanocomposites. (B) Thermopower measurements for pressed pellets of Li_xRuCl_3 ($x \sim 0.2$) and several nanocomposites.

$Li_x(PEO)_yRuCl_3$, $(PANI)_xRuCl_3$, and $(PPY)_xRuCl_3$ are thermally activated, see Figure 4A. In the case of α-$RuCl_3$, Li_xRuCl_3, and $Li_x(PEO)_yRuCl_3$, the $\log(\sigma)$ versus $1/T$ plots are almost linear. The activation energies, which are calculated according to the formula $\sigma = \sigma_0 e^{-\Delta E/2kT}$, are 0.36, 0.30, and 0.35 eV, respectively. Since the pellets used in measurements have interparticle boundaries, the activation energies do not necessarily correspond to the intrinsic band gaps. In $(PANI)_xRuCl_3$ and $(PPY)_xRuCl_3$, the data do not form straight lines in the $\log(\sigma)$ versus $1/T$ plots, which suggests that more than one kind of electrical barriers exist in these materials, including electron hopping barriers associated with transport through and across the chains of the conjugated polymer. At temperatures higher than 100 K, the data of $(PANI)_xRuCl_3$ and $(PPY)_xRuCl_3$ almost fall in straight lines in the $\log(\sigma)$ versus $1/T$ plots. The apparent activation energies are 0.18 eV for $(PANI)_xRuCl_3$ (>125 K) and 0.10 eV for $(PPY)_xRuCl_3$ (>160 K).

The thermopower, which is less sensitive to grain boundary effects, was measured for Li_xRuCl_3 ($x \sim 0.2$), $(PANI)_xRuCl_3$, and $(PPY)_xRuCl_3$, see Figure 4B. All three materials have positive Seebeck coefficients suggesting that the dominant carriers are holes. The p-type charge-transport behavior is consistent with the fact that the reduced $RuCl_3$ layers, the polyaniline (emeraldine salt), and polypyrrole are all p-type conductors. Both the high Seebeck coefficient value of ~60 μV/K for Li_xRuCl_3 and its decreasing trend with rising temperature indicate that Li_xRuCl_3 is a type of semiconductor. The hole type transport in the $[RuCl_3]^{x-}$ layer arises from the partially empty band composed of t_{2g} type Ru orbitals that has an electron configuration between t_{2g}^5 and t_{2g}^6. $(PANI)_xRuCl_3$ and $(PPY)_xRuCl_3$ have lower thermopower values than Li_xRuCl_3, which increase as the temperature increases. This trend is usually seen in metallic conductors. Considering that the reduced $RuCl_3$ layers are thermally activated hopping conductors, the bulk metal-like conductivity, as suggested by the small thermopower of $(PPY)_xRuCl_3$ and $(PANI)_xRuCl_3$, indicates that charge transport in these materials is controlled by the conductive polymers.

5. Magnetic Susceptibility. In α-$RuCl_3$ the intralayer Ru^{3+} ions are ferromagnetically coupled; however, between layers the coupling is antiferromagnetic (AF).[30] The interlayer AF coupling is observable at low temperatures (2−20 K), and causes a well-defined ordering at about 15.6 K, see Figure 5A. At higher temperatures (50−300 K), the magnetic susceptibility follows Curie−Weiss law. The Weiss constant θ is positive which reflects the weak effect of the intralayer ferromagnetic coupling.

In Li_xRuCl_3 ($x \sim 0.2$), the conspicuous AF ordering disappears and the magnetic susceptibility follows Curie−Weiss law to temperatures as low as 2 K, see Figure 5B. We find that a temperature-independent diamagnetic correction (χ_{TIP}) is necessary before the Curie−Weiss law behavior is clearly revealed. The Weiss constant θ becomes negative, indicating a change to a weak overall AF coupling. These changes in magnetic behavior are due to the replacement of Ru^{3+} centers for diamagnetic Ru^{2+} centers in the Ru sublattice, which alters the magnetic couplings both in the layers and between the layers. The magnetic susceptibility data for $Li_x(PEO)_yRuCl_3$, $(PANI)_x$-$RuCl_3$, and $(PPY)_xRuCl_3$ are similar to those of Li_xRuCl_3, see Figure 5C,D. Since the reduction of the $RuCl_3$ layers has already disrupted the original interlayer AF coupling, the subsequent insertion of the polymers does not have any additional effect on the magnetic susceptibility.

The magnetic moment μ_{eff} for α-$RuCl_3$ is 2.32 μ_B (literature value 2.25 μ_B),[30] while those for Li_xRuCl_3 and nanocomposites $Li_x(PEO)_yRuCl_3$, $(PANI)_xRuCl_3$, and $(PPY)_xRuCl_3$ range from 1.6 to 1.74 μ_B. The drop in magnetic moment is due to the decrease in the number of unpaired electrons in $RuCl_3$ layers because of the presence of diamagnetic low-spin Ru^{2+} centers. The paramagnetic moments μ_{eff} and Weiss constants θ for these compounds are listed in Table 1. The magnetic susceptibilities χ_{dia} (diamagnetic contribution of all atoms) and χ_{TIP} (temperature-independent paramagnetism) used in the manipulation of the magnetic data are given in Table 1.

(30) Kobayashi, Y.; Okada, T.; Asai, K.; Katada, M.; Sano, H.; Ambe, F. *Inorg. Chem.* **1992**, *31*, 4570.

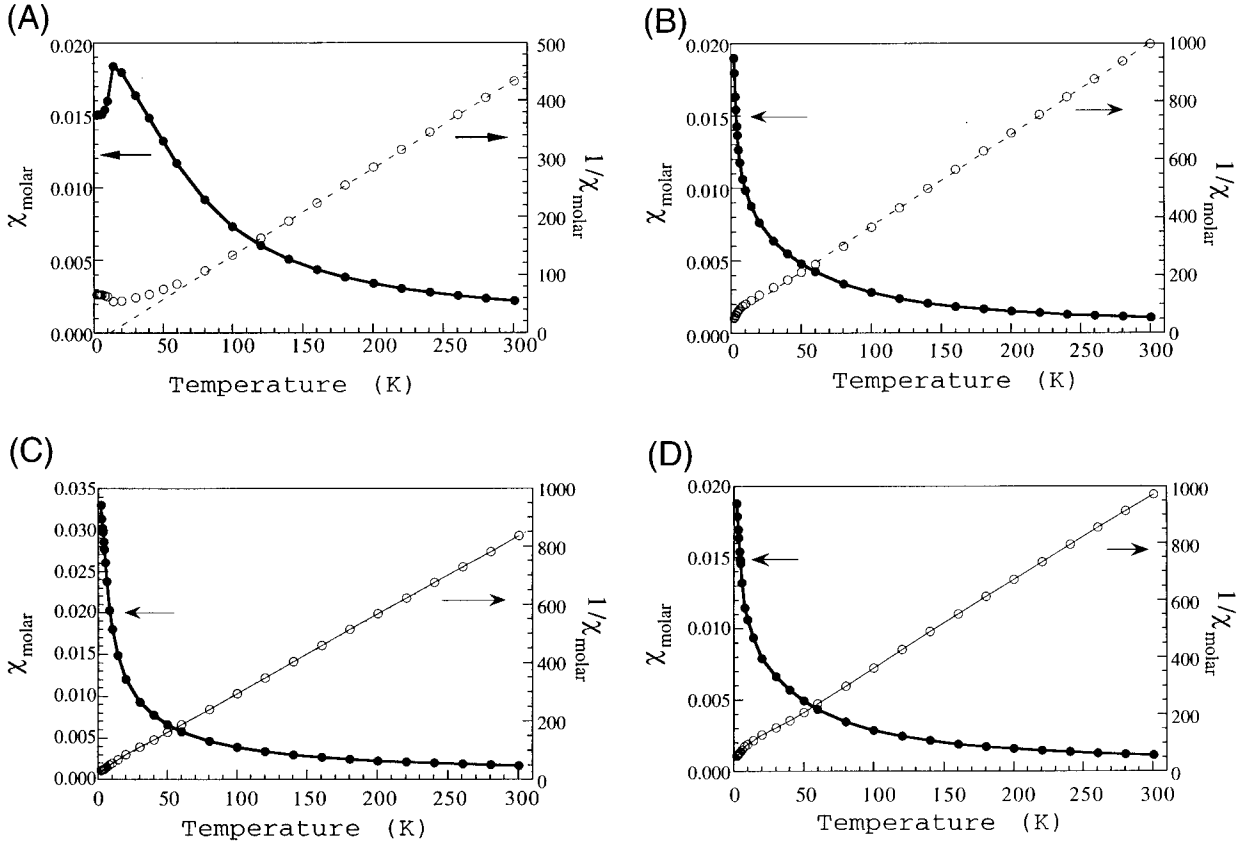

Figure 5. Magnetic susceptibility data as a function of temperature for (A) α-$RuCl_3$, (B) Li_xRuCl_3 ($x \sim 0.2$), (C) $Li_x(PEO)_yRuCl_3$, and (D) $(PANI)_xRuCl_3$.

Table 1. Magnetic Properties of α-$RuCl_3$ and Nanocomposites

sample	μ_{eff} (μ_B/mol Ru)	θ (K)	$10^6\chi_{dia}$ (L/mol Ru)	$10^6\chi_{TIP}$ (L/mol Ru)
α-$RuCl_3$	2.32	11	−101	0
Li_xRuCl_3 ($x \sim 0.2$)	1.60	−18	−101	176
$(PANI)_xRuCl_3$	1.63	−20	−133	250
$Li_x(PEO)_yRuCl_3$	1.73	−10	−167	667
$(PPY)_xRuCl_3$	1.74	−15	−142	247

6. Polymer Structure: One-Dimensional Electron Density Calculations and Arrangement of Polymer Chains in $Li_x(PEO)_yRuCl_3$. In lamellar inorganic/polymeric nanocomposites, the atomic arrangement in the inorganic layers is well-defined. However, the arrangement of polymer chains in the interlayer galleries is not so clear and in general cannot be deduced form the extent of the interlayer expansion alone. The structural issue in these materials is critical if we are to gain better understanding of the properties. Because the interlayer gallery provides a well-defined two-dimensional confinement space for polymer chains, their arrangement, conformation, and dynamic behavior in the gallery is an outstanding issue in fundamental polymer physics. Many have explored such systems with different approaches.[31]

Because of the simple repeat structure and flexible chain of PEO, its intercalative nanocomposites have been the subject of most investigations,[31c−f] yet the structure and conformation of the confined polymer remains an important question. This is due to the relatively few studies aimed at specifically answering structural issues, and due to the fact that the PEO conformation and packing varies from host to host.

Many structures for PEO and PEO complexes are known. The helical conformation is the most common for bulk PEO,[32] and exists in pure spherulite samples.[33] The planar zigzag conformation has been observed in stretched PEO samples.[34] Two more types of conformations have been found in PEO−$HgCl_2$ complexes.[35,36] There are many PEO−(alkali metal salt) complexes with versatile morphologies and the determination of their structures has been attempted. The conformation of PEO in these alkali metal salt complexes is thought to be a double helix,[37] a waving single helix, which accommodates itself around the alkali ion lattice,[38] or one similar to that in the type-II PEO−$HgCl_2$ complex.[39] In addition, many PEO complexes form with organic molecules: PEO−urea complex,[40] PEO−thiourea complex,[41] PEO−*p*-dibromobenzene complex,[42] and PEO−*pa*-nitrophenol complex.[43] Several common PEO conformations are shown in Figure 6. Are any of these structures and conforma-

(31) (a) Nazar, L. F.; Zhang, Z.; Zinkweg, D. *J. Am. Chem. Soc.* **1992**, *114*, 6239. (b) Aranda, P.; Ruiz-Hitzky, E. *Chem. Mater.* **1992**, *4*, 1395. (c) Nazar, L. F.; Wu, H.; Power, W. P. *J. Mater. Chem.* **1995**, *5*, 1985. (d) Liu, Y.-J.; Schindler, J. L.; DeGroot, D. C.; Kannewurf, C. R.; Hirpo, W.; Kanatzidis, M. G. *Chem. Mater.* **1996**, *8*, 525. (e) Matsuo, Y.; Tahara, K.; Sugie, Y. *Carbon* **1997**, *35*, 113. (f) Kerr, T. A.; Wu, H.; Nazar, L. F. *Chem. Mater.* **1996**, *8*, 2005.

(32) (a) Takahashi, Y.; Tadokoro, H. *Macromolecules* **1973**, *6*, 672. (b) Brandrup, J.; Immergut, E. H. *Polymer Handbook*, 3rd ed.; John Wiley & Sons: New York, 1989, pp VI/72.

(33) Price, F. P.; Kilb, R. W. *J. Polym. Sci.* **1962**, *57*, 395.

(34) Takahashi, Y.; Sumita, I.; Tadokoro, H. *J. Polym. Sci., Polym. Phys. Ed.* **1973**, *11*, 2113.

(35) (a) Blumberg, A. A.; Pollack, S. S. *J. Polym. Sci., Part A* **1964**, *2*, 2499. (b) Ishihara, H.; Saito, Y.; Ishihara, H.; Tadokoro, H. *J. Polym. Sci., A-2* **1968**, *6*, 1509.

(36) Yokoyama, M.; Ishihara, H.; Ishihara, H.; Tadokoro, H. *Macromolecules* **1969**, *2*, 184.

(37) Parker, J. M.; Wright, P. V.; Lee, C. C. *Polymer* **1981**, *22*, 1305.

(38) (a) Chatani, Y.; Okamura, S. *Polymer* **1987**, *28*, 1815. (b) Lightfoot, P.; Mehta, M. A.; Bruce, P. G. *Science* **1993**, *262*, 883. (c) Lightfoot, P.; Nowinski, J. L.; Bruce, P. G. *J. Am. Chem. Soc.* **1994**, *116*, 7469.

(39) Chatani, Y.; Fujii, Y.; Takayanagi, T.; Honma, A. *Polymer* **1990**, *31*, 2238.

(40) Tadokoro, H.; Yoshihara, T.; Chatani, Y.; Murahashi, S. *J. Polym. Sci. B* **1964**, *2*, 363.

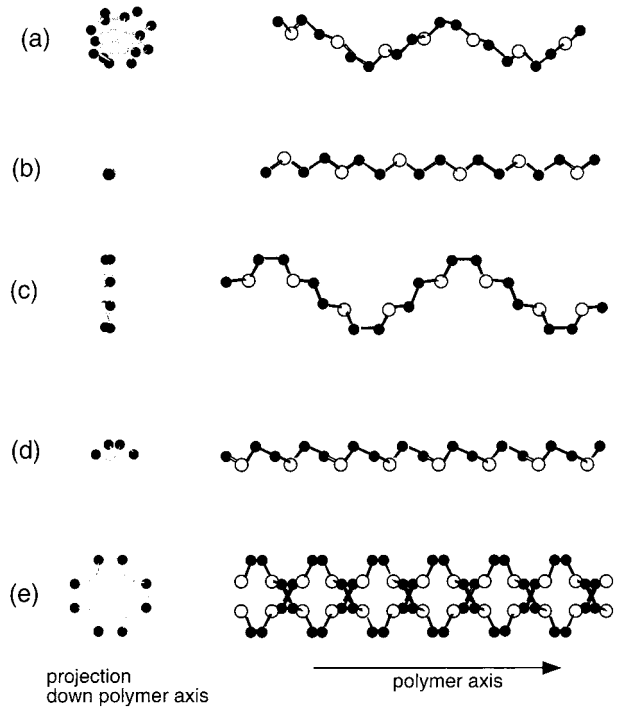

Figure 6. Experimentally observed PEO conformations: (a) single heLi$_x$ (7/2), (b) zigzag, (c) type-I PEO−$HgCl_2$, (d) type-II PEO−$HgCl_2$,- and (e) double helix.

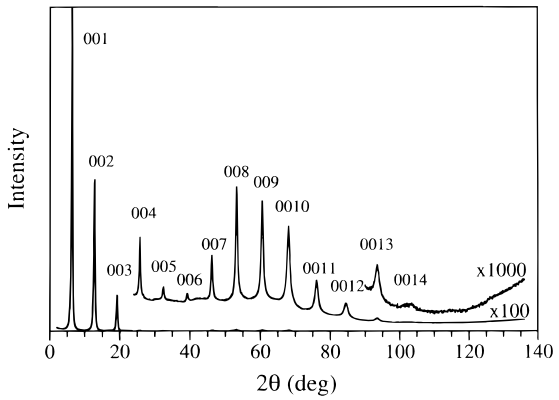

Figure 7. X-ray powder diffraction pattern of an oriented $Li_x(PEO)_y$-$RuCl_3$ film used for the calculation of one-dimensional electron density maps. Due to the preferential orientation of the layers on the sample holder, the reflection-mode powder XRD patterns show predominantly the 00*l* reflections.

tions relevant to the PEO-nanocomposites described here? To answer this question we performed a careful analysis of the XRD reflectivity patterns of well-oriented samples. From these patterns we obtained one-dimensional electron density map profiles projected along the stacking axis (defined as the *c*-axis) and compared them with those profiles expected from the known conformations.

Oriented films of $Li_x(PEO)_yRuCl_3$ have well-defined sharp XRD patterns with up to fourteen 00*l* reflections corresponding to a resolution of 0.98 Å, see Figure 7. The 1-D ED maps for $Li_x(PEO)_yRuCl_3$, which can provide information about the projected structure on the *c*-axis, were calculated from the X-ray powder pattern of oriented films (see Figure 8[44]). In the

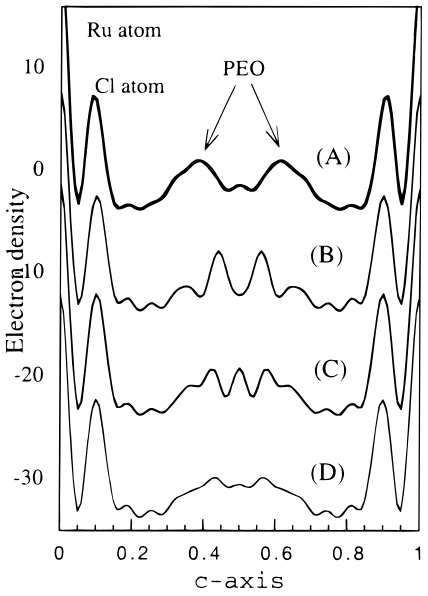

Figure 8. One-dimensional electron density map for $Li_x(PEO)_y$-$RuCl_3$: (A) calculated from XRD data (B) using a model with intragallery double helical PEO that takes an orientation as shown in Figure 6e and (C) using an intragallery double helical PEO model that assumes an orientation of 45° rotation relative to the one shown in Figure 6e and (D) a model with randomly rotated intragallery double helical PEO.

calculation for the 1-D ED map, the phases of the structure factors are needed. Approximate starting phases for the calculation were obtained from the positions of the Ru and Cl atoms. Due to the minor contribution of the polymer to the total scattering intensity, the inorganic layer plays a critical role here in phasing the structure factors and consequently in the computation of the electron density map. Figure 8B,C,D simply provides expected 1D ED profiles based on known models of PEO conformation. Figure 8A shows the 1D ED map calculated from the diffraction data using starting phases.

The 1-D ED map profile for $Li_x(PEO)_yRuCl_3$, projected along the stacking *c*-axis, shows clearly that the electron density due to the guest molecules forms two asymmetric peaks placed 1.4 Å above and below the center of the gallery (Figure 8A). The 1-D ED map suggests that two layers of PEO exist in the gallery, one above and the other below the middle of the gallery. In each layer, the PEO chains seem to adopt a conformation very similar to that of the type-II $HgCl_2$ complex.[45] (The model is shown in Figure 6.) The wide valley in the 1-D ED map in the center of the gallery immediately *excludes the possibility of a layer of helically formed PEO*, which must have appreciable electron density in the central region of the gallery. Considering that the gallery height of $Li_x(PEO)_yRuCl_3$ is 8.0 Å, the accommodation of two layers of helical PEO in such a gallery is also physically impossible, because the van der Waals diameter of one PEO helix is ∼8.0 Å.[32] Furthermore, neither the arrangement of PEO in the zigzag conformation (which was proposed in $(PEO)_xV_2O_5$ [31d]) nor that of the type-I $HgCl_2$ complex (which was proposed for $Na_{0.3}(PEO)_xMoO_3$ [31c]) is consistent with the hereby observed 1-D ED map profile.

(41) Tadokoro, H. *Macromol. Rev.* **1966**, *1*, 119.

(42) Point, J. J.; Coutelier, C. *J. Polym. Sci., Polym. Phys. Ed.* **1985**, *23*, 231.

(43) (a) Point, J. J.; Damman, P. *Macromolecules* **1992**, *25*, 1184. (b) Damman, P.; Point, J. J. *Macromolecules* **1994**, *27*, 3919.

(44) 1-D ED maps were also calculated for models with PEO in zigzag and type-I PEO−$HgCl_2$ conformations. These calculated maps do not match the experimental data and are not presented.

(45) This conformation was also suggested for poly(ethylene glycol) (PEG) in kaolinite/PEG nanocomposites, because its hydrophilic side has higher affinity for the highly polar gibbsite $Al(OH)_3$ side of the clay, whereas its hydrophobic side prefers the not so polar tetrahedral SiO_2 side. Tunney, J. J.; Detellier, C. *Chem. Mater.* **1996**, *8*, 927.

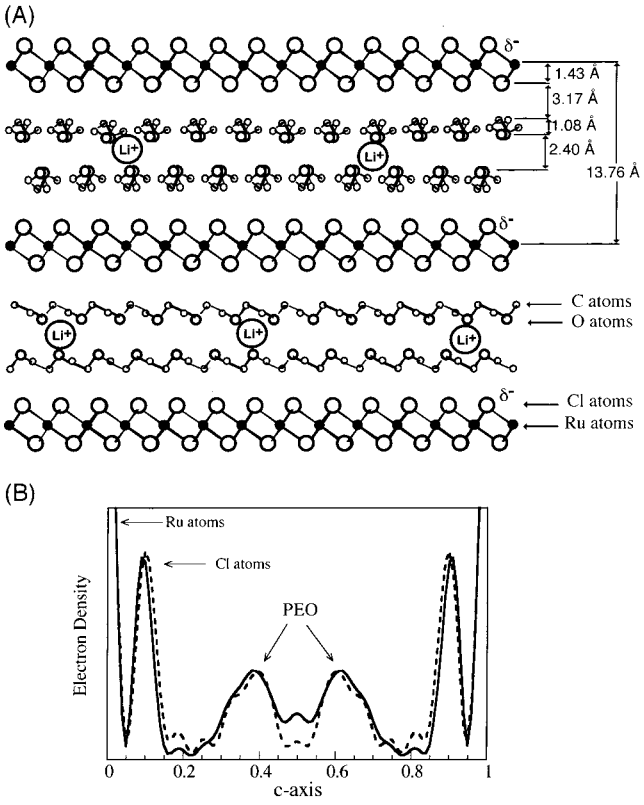

Figure 9. (A) Structural model for $Li_x(PEO)_yRuCl_3$ derived from the one-dimensional electron density maps of $Li_x(PEO)_yRuCl_3$. For clarity, in the two galleries the directions of the PEO are drawn orthogonal to each other. This model should not be taken to mean that a regular periodic arrangement is present in the *ab*-plane. Certainly substantial disorder and lack of registry between these chains is expected. (B) Comparison between the electron density map derived from the proposed model and a map calculated from XRD data of $Li_x(PEO)_y$-$RuCl_3$.

On the basis of the above considerations, the model of Figure 9 can be proposed in which the PEO chains are placed at a van der Waals distance from the $RuCl_3$ layers, i.e., it is in touch with $RuCl_3$. The van der Waals thickness of a layer of α-$RuCl_3$ is 5.73(3) Å. According to the crystal structure of the type-II $HgCl_2$ complex,[34] the distance of the outmost C atom in PEO to the van der Waals boundary of the molecule should be about 1.73 Å. Therefore, the distance of the C atoms should be 4.60 Å from the Ru layer, and the distance of the O atoms from the middle of the gallery is ∼1.20 Å. As shown in Figure 8A, the 1-D ED map profile of the model matches well that calculated from experimental data in all regions except the center of the gallery. This model should not be taken to mean that a regular periodic arrangement is present in the *ab*-plane. Certainly substantial disorder and lack of registry between these chains is expected. Furthermore, the data are not adequate to preclude small contributions from other PEO forms.

In the center of the gallery, the electron density of the model is obviously lower than that suggested from the experimental data due to the fact that disordered water molecules and lithium ions accumulate in this region between the PEO layers. The fact that all the O atoms in the PEO face toward the center of the gallery makes this region hydrophilic, suggesting that it is the most probable location for the Li^+ ions.

Electron density due to the Li^+ ions themselves is not observable in these ED maps due to the small quantities of this very light metal in the material. The validity of the argument that the lithium ions could be in the center of the gallery was

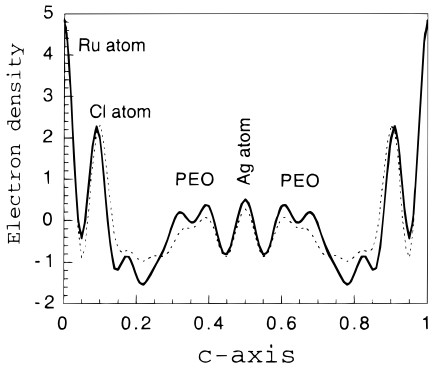

Figure 10. One-dimensional electron density map for $Ag_x(PEO)_yRuCl_3$ using a model similar to that shown in Figure 9. (Solid line, calculated from experimental data; dash line, from model.)

examined by conducting a control experiment in which the Li^+ ions were replaced with Ag^+ ions. We reasoned that because both ions are single-charged the heavier Ag^+ may behave similarly to Li^+ in the nanocomposite and at the same time substantially contribute to the diffraction pattern (i.e. isomorphous replacement). The 1-D ED map for the $Ag_x(PEO)_yRuCl_3$ ($x \sim 0.2$; $y \sim 0.7$)[46] sample indicated substantially higher electron density in the central region, see the central peak in Figure 10. To calculate the expected 1D ED map (dashed line), 0.2 equiv of Ag^+ ions were placed in the center of the gallery. The good agreement between the two maps supports the argument that the ions tend to occupy the center of the gallery.

There exists some similarity between the present model and the structure of the PEO−NaSCN complex, in which PEO also has a conformation similar to that found in type-II PEO−$HgCl_2$.[38] In PEO−NaSCN, the chains are arranged with the CH_2-CH_2 units in proximity of the S atoms of NaSCN, which are less hydrophilic, whereas O atoms coordinate with the Na^+ ions, which are much more hydrophilic. By comparison, PEO in $Li_x(PEO)_yRuCl_3$ behaves similarly by placing its $-CH_2CH_2-$ segments close to the Cl ion surface of the layers while maximizing Li- - -O interactions. In addition, this particular form of PEO−NaSCN complex exists under high tension and converts to another form with a helical PEO conformation if the tension is released. In $Li_x(PEO)_yRuCl_3$, the polymer chains extend themselves over a 2-D environment, which of course represents a form of tension as well.

The proposed $Li_x(PEO)_yRuCl_3$ model of Figure 9 matches well the observed 1-D ED map and is geometrically and chemically reasonable. This model is different from the one proposed for the Li/PEO/montmorillonite nanocomposite in which the Li^+ ions are thought to be located near the surface oxides of the silicate layer.[47] Presumably the lower affinity of Li^+ for Cl^- causes it to select the middle of the gallery, which presents an oxygen-rich coordination environment. Such a PEO arrangement should provide a good diffusion environment for ions in directions parallel to the layers, which could make $Li_x(PEO)_yRuCl_3$ a comparable or even better ion-conductor than the amorphous PEO−(alkali-metal) complexes which have segments of helical PEO chains in the structure[48] (see below).

(46) $Ag_x(PEO)_xRuCl_x$ was prepared from Li_xRuCl_3 with a procedure similar to that used for the Li analogue $Li_x(PEO)_xRuClx$ using $AgNO_3$. This is an ion-exchange (Ag^+ for Li^+) reaction where both PEO and $AgNO_3$ are added to the reaction. The $Ag/RuCl_3$ ratio was determined to be 0.2 with EDS analysis. The amount of PEO was determined from C, H, N analysis.

(47) Yang, D.-K.; Zax, D. B. *J. Chem. Phys.* **1999**, *110*, 5325.

(48) Gray, F. M. *Solid Polymer Electrolytes*; VCH Publisher: New York, 1991; Chapter 5, p 83.

7. PEO Conformation from IR Spectra. IR spectroscopy is not a decisive technique to probe the PEO conformation in a nanocomposite. The weakness of IR spectroscopy derives from the uncertainty in correctly assigning the observed signals. Nevertheless, some discussion here is warranted to highlight the differences between the various known forms and the difficulties associated with an unambiguous assignment. The spectral region from 800 to 1000 cm^{-1} is supposed to be sensitive to the conformation of PEO chains. A trans O−C−C−O conformation would have absorption peaks around 773 and 992 cm^{-1}, while a gauche O−C−C−O conformation would have absorptions around 880 and 944 cm^{-1}.[49] All known PEO conformations, however, only have absorptions around 850 and 950 cm^{-1}, even those in type-I PEO−$HgCl_2$ complex[35b] and PEO−*p*-nitrophenol complex,[43b] in which the trans O−C−C−O exists. Less is known about amorphous versions.

In addition, some controversy in the PEO IR peak assignment arises from the disagreement among the type-I PEO−$HgCl_2$ IR data reported.[35a,b] The peaks observed at 1324, 1309, 1014, and 815 cm^{-1} [35a] were assigned to the trans O−C−C−O conformation,[49,31c] because there were no corresponding peaks in the IR spectra of bulk PEO. The more recent IR spectra, reported for type-I PEO−$HgCl_2$, [35b] did not have peaks at 1309, 1014, and 815 cm^{-1}, while the spectra of type-II PEO−$HgCl_2$ had peaks at 1312 and 1015 cm^{-1}.[35b] Recalling the fact that the type-I PEO−$HgCl_2$ converts to type-II PEO−$HgCl_2$ spontaneously,[35b] one might suspect that the type-I PEO−$HgCl_2$ sample used by Blumberg and Pollack[35a] also contained type-II PEO−$HgCl_2$. If this is so, the peaks at 1309 and 1014 cm^{-1} do not belong to the trans O−C−C−O conformation. Therefore, 1324 cm^{-1} may be the only peak that can be assigned to the trans O−C−C−O conformation, as is done in some references.[31b,e,f] The spectrum of $Li_x(PEO)_yRuCl_3$ does not have a peak near 1324 cm^{-1}, see Figure 4C, which suggests that no trans O−C−C−O conformation exists. This agrees with the choice of the type-II PEO−$HgCl_2$ conformation proposed in the previous section. However, IR spectroscopy alone is not adequate to unambiguously select which conformation is present.

Absorption peaks of $Li_x(PEO)_yRuCl_3$ are compared in Table 2 with those of helical PEO, type-I PEO−$HgCl_2$, and type-II PEO−$HgCl_2$ read from the spectra in red 35b.[50] For easier comparison the peaks have been grouped into regions I through VII in Table 2. The IR spectrum of $Li_x(PEO)_yRuCl_3$, exhibits broader peaks resulting in some adjacent overlap. In regions II and VII, the peaks of $Li_x(PEO)_yRuCl_3$ match those of type-II PEO−$HgCl_2$. The absence of strong peaks at ∼1278 and ∼875 cm^{-1} in the spectrum of $Li_x(PEO)_yRuCl_3$ (see regions III and VII in type-I PEO−$HgCl_2$) suggests that a type-I-like form of the polymer is probably not present in significant amounts in the nanocomposite.

In region IV, the broad peak at 1094 cm^{-1} matches the 1100 cm^{-1} peak of the type-II PEO−$HgCl_2$. The peak is assigned to C−O stretching and its slight shift to the lower frequency is caused by the coordination of O atoms to Li^+ ions. The peak at 1154 cm^{-1} in type-II PEO−$HgCl_2$ is weak, so it does not appear in the IR spectrum of $Li_x(PEO)_yRuCl_3$. Type-II PEO−$HgCl_2$ has a pair of peaks in both regions III and V (see Table 2), while $Li_x(PEO)_yRuCl_3$ has only one peak in each of them. In the spectrum of type-II PEO−$HgCl_2$, the two peaks in each pair have a difference of 31 cm^{-1} or less. Each pair might merge to give a single peak in the nanocomposite spectrum. Some of the peaks observed in the type-II conformation may be due to modes associated with Hg^{2+} ion binding (absent in the nanocomposite) and may not appear in the spectrum of $Li_x(PEO)_yRuCl_3$.[51]

Table 2. A Comparison of IR Absorptions (cm^{-1}) of PEO in Various Forms

$Li_x(PEO)_{1.5}RuCl_3$ ($x \sim 0.5$)	pure PEO	PEO·$HgCl_2$(I)	PEO·$HgCl_2$(II)	region
1465 (w)	1462 (s)	1468 (s)		
1455 (w)	1456 (w)	1451 (s)		I
1445 (w)			1445 (s)	
1352 (w)	1355 (w)	1350 (s)	1356 (m)	II
1303 (w)	1338 (s)	1328 (m)	1312 (s)	
	1278 (s)	1278 (s)		
			1262 (m)	III
1248 (w)		1246 (s)		
	1237 (m)		1239 (s)	
	1143 (vs)[a]		1154 (m)	IV
1094 (vs)	1110 (vs)[a]	1110 (vs)	1100 (vs)	
1060 (sh)		1064 (s)		
	1057 (s)	1044 (s)	1046 (vs)	V
1031 (m)		1032 (s)	1015 (vs)	
950 (m)	950 (s)	945 (s)	944 (w)	
920 (sh)			923 (s)	VI
			892 (m)	
		876 (s)		
846 (m)		859 (m)		VII
	837 (s)[a]	831 (m)	835 (s)	

[a] The peaks around 1148, 1112, and 851 cm^{-1} are characteristic of the helical PEO conformation: Matsuura, H.; Miyazawa, T. *Spectrochim. Acta* **1967**, *23A*, 2433.

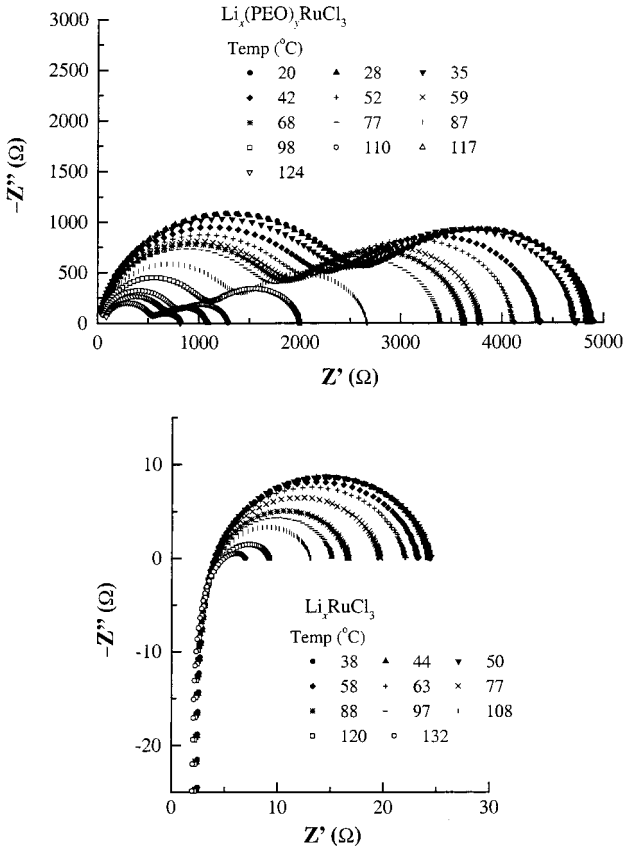

Figure 11. Impedance plots for $Li_x(PEO)_yRuCl_3$ (top) and $Li_{0.2}RuCl_3$ (bottom) at different temperatures.

8. Ionic Conductivity. Intercalation electrodes and polymer electrolytes have been central topics in solid-state ionics for more than 20 years.[52] Ion conductivity plays an important role

(49) Papke, B. L.; Ratner, M. A.; Shriver, D. F. *J. Phys Chem. Solids* **1981**, *42*, 493.

(50) Reference 35b provides the spectra of two orientations with the electric vector perpendicular and parallel to the fiber axes. A spectrum from an un-oriented sample should correspond to the superposition of the two spectra.

in both types of materials. Since lamellar nanocomposites which contain PEO can be used for both intercalation electrodes and polymer electrolytes, ionic conductivity is an important property to investigate.

The complex impedance ($Z^* = Z^* - iZ^{**}$) spectra for $Li_{0.2}(PEO)_xRuCl_3$ and for comparison $Li_{0.2}RuCl_3$ were measured between 20 and 130 °C. The data are presented in Figure 11. The spectra for $Li_{0.2}(PEO)_xRuCl_3$ (Figure 11) are composed of two well-separated semicircles whose overall size decreases with increasing temperature. $Li_{0.2}(PEO)_xRuCl_3$ exhibits both ionic and electronic conductivity due to the intercalated Li^+ ions and reduced $[RuCl_3]^{x-}$ layers, so its impedance derives from the combination of the two types of charge transport. The depression of semicircles in Figure 11 (top), with their centers below the Z^* axis, indicates distributed relaxation time constants (τ) involved in the Li^+ conduction, as is expected from the composite structure of $Li_{0.2}(PEO)_xRuCl_3$.

The electronic (σ_{el}) and ionic (σ_{ion}) conductivities of $Li_{0.2}(PEO)_xRuCl_3$, converted from the fitted R_{el} and R_{ion} values, are presented in Figure 12A. As shown in the figure, the ionic conductivity of $Li_{0.2}(PEO)_xRuCl_3$ falls in the range $10^{-4.2}-10^{-3.0}$ S/cm between 20 and 130 °C, and is comparable to those of the best (lithium salt)/polymer electrolytes.[48] The electronic conductivity is of the same order of magnitude in the same temperature range. The contribution of the ionic conductivity to the total electrical conductivity, which is defined as the transference number ($t_{ion} = \sigma_{ion}/(\sigma_{ion} + \sigma_{el})$), is estimated at 0.55−0.43 in the above temperature range. The deflection in the line of the Arrhenius plot, which appears in both the ionic and electrical conductivity, indicates a phase transition at about 80 °C. The corresponding activation energies below and above the transition temperature are 0.146 and 0.485 eV for σ_{ion} and 0.082 and 0.488 eV for σ_{el}.

The corresponding impedance spectra for $Li_{0.2}RuCl_3$ indicate different transport properties for this material. First, their significantly lower impedance values correspond to electrical conductivities about 2 orders of magnitude higher, see Figure 11 (bottom). Second, they are composed of only one semicircle and the vertical tail extends across the Z^* axis, in contrast to those of $Li_{0.2}(PEO)_xRuCl_3$.

In $Li_{0.2}RuCl_3$, σ_{el} is so much higher than σ_{ion} that the total electrical conductivity σ_{Tot} is practically equal to σ_{el}. Thus σ_{ion} could not be extracted from σ_{Tot}. As a consequence, σ_{ion} is estimated to be much lower than that of $Li_{0.2}(PEO)_xRuCl_3$.[53] The σ_{el} (σ_{Tot}) of $Li_{0.2}RuCl_3$, which is also thermally activated, is plotted together with the σ_{el} and σ_{Tot} of $Li_{0.2}(PEO)_xRuCl_3$ in Figure 12B. The agreement with the electrical conductivity values determined independently with the four-probe method, as discussed above, is excellent. The comparison shows that *the encapsulation of insulating PEO results in a substantial increase in ionic mobility of Li*. The decrease in σ_{el} (with respect to $Li_{0.2}RuCl_3$) is attributed mainly to the increased separation in the $[RuCl_3]^{x-}$ layers. The presence of PEO in the galleries provides for low activation energy barriers for Li^+ transport, which is believed to occur primarily through two-dimensional channels.

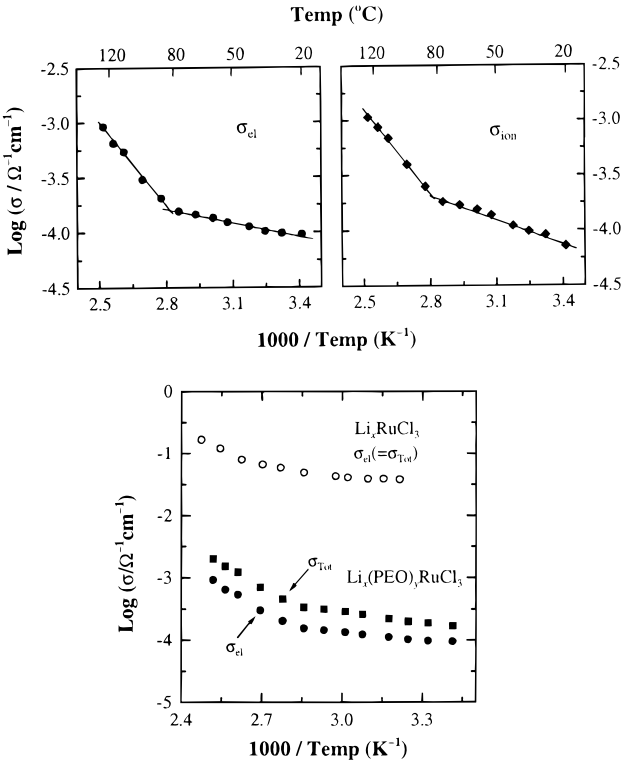

Figure 12. (Top) Arrhenius plots of the ionic (right) and electronic (left) conductivities of $Li_x(PEO)_yRuCl_3$. (Bottom) Comparison of the electronic conductivity of Li_xRuCl_3 with the electrical (σ_{Tot}) and electronic conductivities of $Li_x(PEO)_yRuCl_3$, measured by impedance spectroscopy.

Concluding Remarks

The robustness of α-$RuCl_3$, in acidic or basic aqueous solutions, and its good stability against reducing and oxidizing conditions makes it an excellent compound for intercalation reactions. This is a rare set of properties among transition metal halides. The insertion of conducting polymers PANI and PPY and the water-soluble polymers PEO, PVP, and PEI in $RuCl_3$ gives a new class of lamellar (metal halide)/polymer intercalative nanocomposites. The synthesis of these nanocomposites is enabled mainly by the successful exfoliation of α-$RuCl_3$ after controlled lithiation, which allows the use of the encapsulative precipitation method.[10] On the other hand, α-$RuCl_3$ is also one of the few layered hosts that is suitable for in situ redox intercalative polymerization, and provides an interesting and unique metal halide component for new nanocomposites.

α-$RuCl_3$ nanocomposites contain reduced layers in which free electron hopping, associated with Ru^{2+}/Ru^{3+} couples, raises the

(51) The IR absorption of $Li_x(PEO)_yRuCl_3$ in regions I and VI is different from that of type-II PEO−$HgCl_2$ than in other regions. The peaks of $Li_x(PEO)_yRuCl_3$ at 1465, 1455, and 950 cm^{-1}, which are close to those of the helical PEO, may come from PEO chains dangling outside the layers. (Other absorption peaks of free PEO chains may be buried in the absorption of $Li_x(PEO)_yRuCl_3$.) In region VI, the absence of the 892 and 944 cm^{-1} peak in the $Li_x(PEO)_yRuCl_3$ spectrum might be explained by its low intensity. The absorption in this region is contributed mostly by the 950 cm^{-1} peak of the free PEO chains and the 923 cm^{-1} peak of the type-II PEO−$HgCl_2$ conformation. In any case, the IR absorption profile of $Li_x(PEO)_yRuCl_3$ seems to match the spectrum derived from a superposition of the absorption peaks of type-II PEO−$HgCl_2$ conformation and free PEO chains.

(52) Bruce, P. G. In *Fast Ion Transport in Solids*; Scrosati, B., et al., Eds.; NATO ASI Ser. Ser. E; Kluwer Academic Pub.: Dordrecht, The Netherlands, 1993; Vol. 250, p 87.

(53) As an alternative method to determine the ionic conductivity of Li_x-$RuCl_3$, a DC relaxation technique could be useful, since in principle it can provide the impedance spectrum information at the extremely low ω region (≪5 Hz). DC polarization−relaxation measurements for $Li_{0.2}RuCl_3$ were tried with a cell in the configuration "stainless steel/Li_x/sample/stainless steel", with various polarization voltages and times, and with various lithium salts (LiI, $Li(CF_3SO_2)_2N$, and $LiClO_4$). Nevertheless, we could not observe a proper relaxation behavior for the specimen, which is probably due to a systematic limitation arising from the very low σ_{ion} of Li_xRuCl_3. An ideal DC relaxation experiment can be performed by an application of the electron-blocking compartment with very high σ_{ion}, but as far as we know, such Li^+ conductors are not readily available yet.

electrical conductivity by 2−3 orders of magnitude. The intercalation of conducting polymers can further increase the conductivity. The dominant carriers in the $[RuCl_3]^{x-}$ layers are holes residing in a narrow t_{2g}-type band. The reduction of α-$RuCl_3$ and polymer insertion profoundly affect the intralayer and interlayer Ru^{3+} magnetic couplings, so that new magnetic properties appear in the nanocomposites.

On the basis of X-ray scattering and IR spectroscopy, a structural model is proposed for $Li_x(PEO)_yRuCl_3$, in which each gallery contains two layers of PEO chains in a conformation similar to that found in type-II PEO−$HgCl_2$. The Li^+ ions seem to reside exactly in the middle of the interlayer space sandwiched between two monolayers of PEO. The model suggests that $Li_x(PEO)_yRuCl_3$ should have good two-dimensional ionic conductivity, which is indeed confirmed by impedance spectroscopy. In fact, the ionic conductivity is comparable to those of the best (lithium salt)/polymer electrolytes. Given that the materials in the general class of polymer/$RuCl_3$ combine high electrical conductivity (e.g. conjugated polymer guests) with the potential catalytic properties of $RuCl_3$, it is intriguing to contemplate new systems with valuable electrocatalytic properties.

Acknowledgment. Financial support from the National Science Foundation is gratefully acknowledged. This work made use of the magnetic measurement facilities of the Department of Physics and the SEM and TEM facilities of the Center for Electron Optics at Michigan State University.

JA9944610